45th SME North American Manufacturing Research Conference, NAMRC 45, LA, USA

Periodic error compensation in fiber-coupled heterodyne interferometry

Chao Lu[a], Ethan D. Burnham-Fay[b], Jonathan D. Ellis[b], Tony L. Schmitz[c], Joshua A. Tarbutton[c]*

[a]*Department of Mechanical Engineering, University of South Carolina, Columbia, SC, 29208, USA*
[b]*Department of Mechanical Engineering and The Institute of Optics, University of Rochester, Rochester, NY, 14627, USA*
[c]*Department of Mechanical Engineering and Engineering Science, University of North Carolina at Charlotte, Charlotte, NC, 28223, USA*

Abstract

This paper extends the application of a novel wavelet-based periodic error compensation algorithm in fiber-coupled heterodyne interferometry. In this case, the amplitudes of periodic error may be fluctuating and traditional digital algorithms are not well-suited. The wavelet-based method, however, has the ability to compensate non-stationary periodic error. In this work, the algorithm is used to compensate periodic error in simulated and experimental constant and experimental non-constant velocity motions and to reduce the error by approximately 80.1%, 81.2% and 68.3%.

1. Introduction

Heterodyne displacement measuring metrology provides high accuracy, long range and high resolution for dimensional metrology. The heterodyne Michelson interferometer is used in a number of non-contact displacement measurement applications including position feedback of lithographic stages for semiconductor fabrication and position calibration for other metrology systems. In the interferometer, the laser source includes two frequencies.

---

* Corresponding author. Tel.: +1-704-687-7213; fax: +1-704-687-8345.
  E-mail address: Joshua.Tarbutton@uncc.edu

The two optical frequencies are separated into one beam to the fixed retroreflector and one to the moving target via polarization. The lights from the two paths are recombined to obtain an interference signal, which results in a measurement signal at the heterodyne (split) frequency of the laser source. The measurement signal is compared to the optical reference signal. Motion in the measurement arm causes a Doppler shift of the heterodyne frequency which is measured as a continuous phase shift that is proportional to displacement. Ideally the two beams are linearly polarized and recombined at the polarizing beam splitter so that only one frequency is directed toward each path. In practice, however, undesirable frequency mixing occurs which yields periodic errors [1-3]. Sources of frequency mixing include non-orthogonality between the linear beam polarization, elliptical polarization of one beam, imperfect optical components, parasitic reflections from the surface, and mechanical misalignment in the interferometer. Typically, both 1st and 2nd order periodic errors occur, which correspond to one and two periods per displacement fringe (a full cycle of phase change, which is also an optical path length change of one wave length, referred to as one "fringe"), as shown in Fig. 1. The periodic error can limit the accuracy of the heterodyne interferometer to approximately the nanometer level.
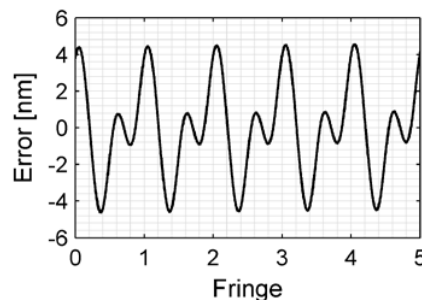
Fig. 1. Example of 1st and 2nd order periodic error as a function of fringes. Typically, 1st order error has a larger magnitude than 2nd order error.

In measurements demanding high accuracy, the thermal errors introduced by heat from the laser head in heterodyne interferometer may become a major error source. The heat may affect the measurement accuracy through changes in ambient temperature or thermal expansion of mechanical components. A fiber coupling between laser head and interferometer optics can solve this problem. It separates the laser head from the interferometer system so the thermal error source is removed. In addition, the use of an optical fiber may reduce the amount of expensive optics required to deliver the beam to the interferometer and may also eliminate the efforts for the alignment between laser head and interferometer optics. However, fiber delivery will inherently decrease polarization stability and add time-varying effects, causing the amplitudes of periodic error to fluctuate [4].

Many studies have investigated the measurement and compensation of periodic error, including frequency domain [5-7] and time domain regression (TDR) approaches [8, 9]. For the frequency domain approach, the periodic error are measured by calculating the Fourier transform of the time domain data collected during constant velocity target displacement. However, this method is not well-suited to non-constant velocity profiles because it always assumes a stationary signal. An alternate TDR digital algorithm which can be applied in real-time for constant or non-constant velocity motions is also available for measuring and compensating 1st and 2nd order periodic error. But this method is not able to compensate periodic error with fluctuating amplitudes.

In this research, a real-time wavelet-based algorithm, which was developed in previous work [10-13], is extended to compensate periodic error with fluctuating amplitudes in both constant and non-constant velocity motions. Previous work addressed systems where periodic error amplitude is always constant in contrast to the present work where the amplitude is varying with time.

2. Background

The wavelet transform can be used to analyze time series data that contains non-stationary (variable period) power at multiple frequencies [14]. Wavelet functions refer to either orthogonal or non-orthogonal wavelets. The

choice of the appropriate wavelet transform (continuous or discrete) and wavelet function is based on whether the purpose of data analysis is detection or compression [15].

A wavelet function $\psi(t)$ is a finite energy function [16] with an average of zero,

$$\int_{-\infty}^{+\infty} \psi(t)\,dt = 0 \tag{1}$$

A wavelet family is generated by dilating the mother wavelet via the scale s and translating it via the location u. This series of wavelets can be expressed as

$$\psi_{u,s}(t) = \frac{1}{\sqrt{s}} \psi\left(\frac{t-u}{s}\right) \tag{2}$$

In this research, a continuous wavelet transform (CWT) is used to analyze the signal $x(t)$, with a wavelet function $\psi(t)$. For a one-dimensional signal $x(t)$, the CWT is defined as the convolution of $x(t)$ with a scaled and translated version of $\psi(t)$ via

$$Wx(u,s) = \int_{-\infty}^{+\infty} x(t)\psi_{u,s}^{*}(t)\,dt = \int_{-\infty}^{+\infty} x(t)\frac{1}{\sqrt{s}}\psi^{*}\left(\frac{t-u}{s}\right)dt \tag{3}$$

where, $\psi^{*}(t)$ = wavelet function, s = scale, and u = location. In the present work, the complex Morlet wavelet is used as the mother wavelet

$$\psi^{*}\left(\frac{t-u}{s}\right) = \pi^{-\frac{1}{4}} e^{i2\pi f_0 \frac{t-u}{s}} e^{-\frac{1}{2}\left(\frac{t-u}{s}\right)^2} \tag{4}$$

The choice of this wavelet is based on its ability to locate the 1st order periodic error frequency at the scale with the maximum wavelet coefficient and to obtain the periodic error phase information using the real and imaginary parts of this coefficient. In practice, Equation 3 must be converted from continuous to discretized form. The discrete time continuous wavelet transform (DTCWT) can be described as:

$$Wx(n,s) = \sum_{n'=1}^{M}\left(x(n')\sqrt{s}\psi^{*}\left(\frac{(n'-n)\Delta t}{s}\right)\Delta t \right) \tag{5}$$

where, $x(n) = n^{th}$ discrete data point, ψ^{*} = mother wavelet, M = number of total data points in the signal, and Δt = sampling time. After applying the complex Morlet wavelet to the signal, the wavelet transform result is a two-dimensional complex array. This array can be used to extract the "ridge" and, therefore, the phase of the periodic errors. The ridge is the location where the wavelet transform coefficient reaches its local maximum along the scale direction [17]; the coefficient is maximum when the analysis frequency equals the signal frequency [18]. The ridge and phase are

$$ridge(n) = \max\left\{ |Wx(n,s)| \right\} \text{ and} \tag{6}$$

$$\phi(n,s) = \arctan\left(\frac{\text{Im}\left(Wx\left(n, s_{ridge}\right)\right)}{\text{Re}\left(Wx\left(n, s_{ridge}\right)\right)}\right) \tag{7}$$

where, s_{ridge} = scale at the ridge, and *Im* and *Re* represent the imaginary and real parts of the CWT coefficients, respectively.

3. Real-time periodic error compensation algorithm

The calculation process of the periodic error compensation algorithm, which can be processed in real-time, is depicted in Fig. 2. Here the algorithm will be briefly described. A detailed description of the algorithm is provided in [13].
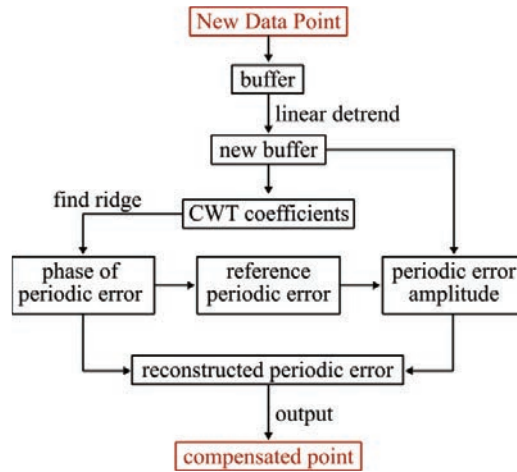
Fig. 2. Calculations to implement the periodic error compensation algorithm.

The algorithm starts with storing the latest N data points in a memory array. A new array is obtained after detrending the measured data in the memory array. The DTCWT (Equation 5) is then applied to the new array. After applying the complex Morlet wavelet to the signal, the resulting wavelet transform is a complex array along the scale direction. The modulus and phase can be calculated using Equations 6 and 7, and the ridge can be determined at scale s_1. This scale corresponds to the 1st order periodic error frequency. Because the scale is inversely related to the frequency, the scale $s_i = s_1/i$ corresponds to the ith order periodic error frequency.

For each new data point, the ridge and phase is calculated, so the periodic error phase information is determined. Arrays for the reference j^{th} order periodic error are constructed,

$$r_j[1\ldots N] = \left\{\sin\left(j\varphi(1)\right), \sin\left(j\varphi(2)\right), \ldots, \sin\left(j\varphi(N)\right)\right\} \tag{8}$$

where, $\varphi[x] = \phi(x, s_{ridge})$. We consider a general form of m order periodic errors,

$$\sum_{j=1}^{m} A_j r_j[1\ldots N] \tag{9}$$

where, $A_j = j^{th}$ order periodic error amplitude. Apply DTCWT linearity property to obtain equations:

$$
\begin{cases}
c_1 = A_1 d_{11} + A_2 d_{12} + \ldots + A_m d_{1m} \\
c_2 = A_1 d_{21} + A_2 d_{22} + \ldots + A_m d_{2m} \\
\quad\quad\quad\quad \vdots \\
c_m = A_1 d_{m1} + A_2 d_{m2} + \ldots + A_m d_{mm}
\end{cases}
\tag{10}
$$

where, c_i = the CWT result for the data array at scale s_i, and d_{ij} = the CWT result for reference j^{th} order periodic error at scale s_i.

Using Equation 10, the amplitudes can be solved. Then m order periodic errors can be reconstructed as,

$$
\sum_{i=1}^{m} A_i \sin\left(i\varphi\left(N\right)\right)
\tag{11}
$$

Finally, this reconstructed periodic error is subtracted from the original displacement data to obtain a compensated data point.

4. Simulations and experiments

To demonstrate the effectiveness of the wavelet-based approach, simulated data was created for a linear displacement of 15 µm (constant velocity of 50 mm/min) with periodic error amplitudes varying in frequency of 50 Hz (sampling frequency was 62.5 kHz), and experimental data of a small stage was collected for a displacement of 50 µm with constant velocity profile (due to constant velocity of 7.14 µm/s), and for a reciprocate motion between 5 µm and -5 µm (constant frequency of 0.1 Hz). Only first and second order periodic errors appear. In this signal, first order error is dominating. The amplitudes of periodic error are fluctuating. The experimental parameters were: 1) He-Ne laser wavelength of λ = 632.99 nm; 2) a fold factor of FF = 2, which describes the number of light passes through the interferometer; and 3) a sampling frequency was 3.788 kHz. A schematic of the fiber-coupled heterodyne interferometer used in the experiments is shown in Fig. 3.
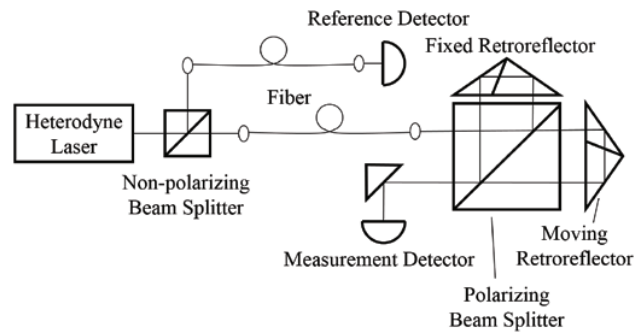
Fig. 3. Schematic of the fiber-coupled heterodyne interferometer.

Fig. 4 displays the simulated displacement and periodic error. The periodic error compensation result is shown in Fig. 5. The root-mean-square (RMS) error is reduced by approximately 80.1%.

Fig. 6 shows the experimental linear displacement and periodic error, which was isolated by subtracting a least square fit polynomial from the displacement signal. The low frequency drift is caused by an imperfect polynomial fit or non-constant acceleration. An example which shows finding the ridge from wavelet transform coefficients at 7 s is displayed in Fig. 7. Along the scaling direction, the maximum coefficient locates at scale 271, which is related to

the first order periodic error frequency. The amplitude identification results are shown in Fig. 8, and the overall periodic error compensation result is displayed in Fig. 9. The RMS error is reduced by approximately 81.2%.
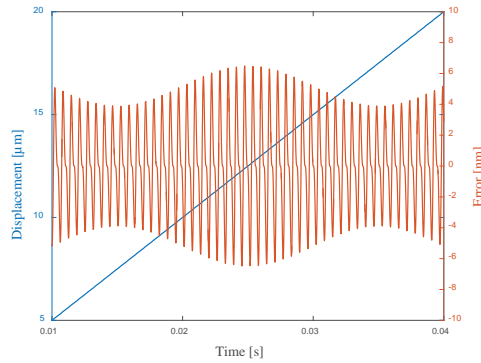
Fig. 4. Simulated displacement and periodic error.
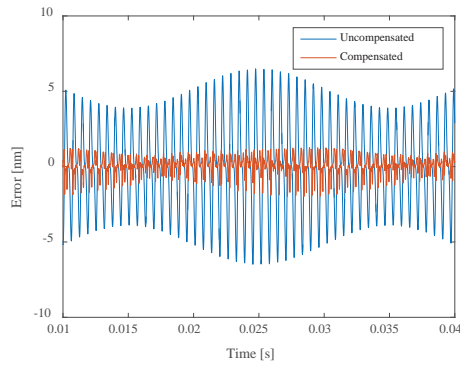
Fig. 5. Periodic error compensation result for the simulated motion.
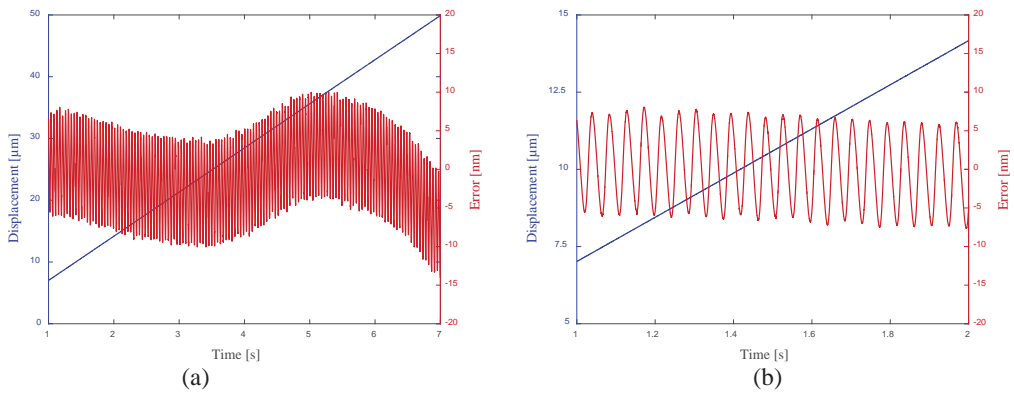
Fig. 6. (a) Experimental linear displacement and periodic error, and (b) zoomed view of the displacement and superimposed periodic error.

Fig. 10 shows the experimental reciprocate motion (non-constant velocity motion) and the superimposed periodic error. The periodic error compensation result is shown in Fig. 11. The RMS error is reduced by approximately 68.3%.
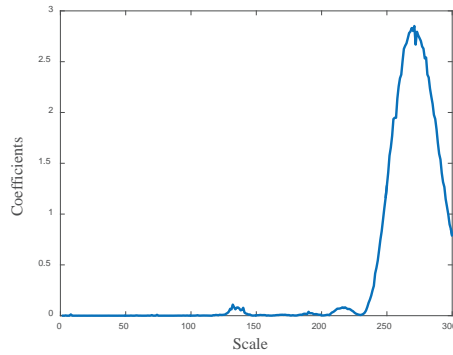
Fig. 7. An example of finding the ridge from wavelet transform coefficients at 7 s.
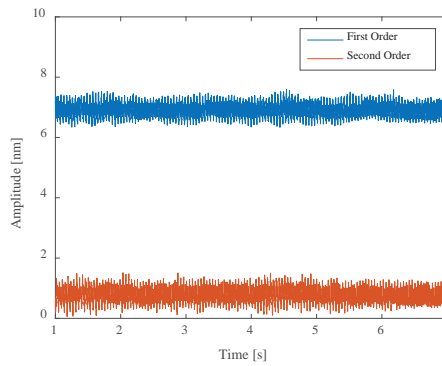
Fig. 8. The measured amplitudes.
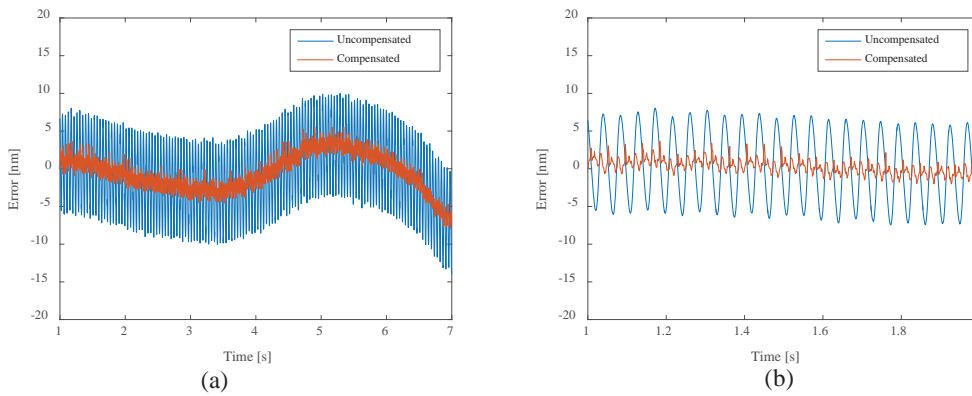
Fig. 9. (a) The result of periodic error compensation for the experimental constant velocity motion, and (b) zoomed view of the compensation result.
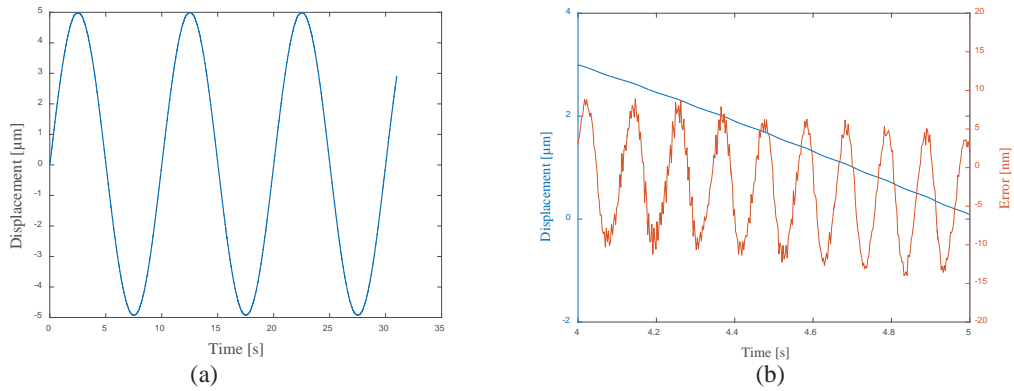
Fig. 10. (a) The experimental reciprocate displacement, and (b) zoomed view of the displacement and superimposed periodic error.
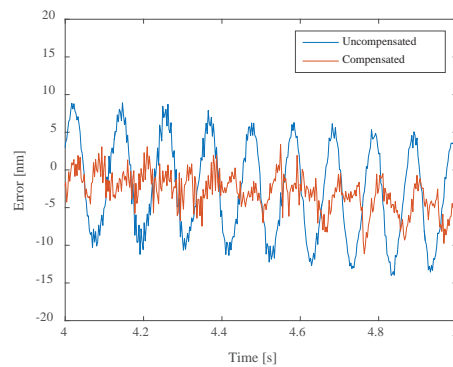
Fig. 11. Periodic error compensation result for the experimental non-constant velocity motion.

5. Conclusions

The wavelet-based periodic error measurement and compensation method is the first to be applied to compensate periodic error with fluctuating amplitudes in fiber-coupled heterodyne interferometer. This is also the first time to use digital measurement in this varying-amplitude periodic error since traditional digital algorithms cannot be applied. The compensation result shows that the wavelet-based algorithm can identify non-stationary periodic error in simulated and experimental constant and experimental non-constant velocity motions and reduce the RMS error by approximately 80.1%, 81.2% and 68.3%, respectively. The success of non-stationary periodic error compensation demonstrates the ability of this wavelet-based approach to compensate periodic error with fluctuating amplitudes.

References

[1] G. Fedotova, Analysis of the measurement error of the parameters of mechanical vibrations. Measurement Techniques, 23(7), (1980) 577-580.
[2] R. Quenelle, Nonlinearity in interferometric measurements. Hewlett-Packard Journal, 34(4), (1983) 10.
[3] C. Sutton, Nonlinearity in length measurements using heterodyne laser Michelson interferometry. Journal of Physics E: Scientific Instrumentation, 20, (1987) 1290-1292.
[4] B.A.W.H. Knarren, S.J.A.G. Cosijns, H. Haitjema, P.H.J. Schellekens, Validation of a single fibre-fed heterodyne laser interferometer with nanometre uncertainty. Precision Engineering, 29(2), (2005) 229-236.

[5] S. Patterson, J. Beckwith, Reduction of systematic errors in heterodyne interferometric displacement measurement. In Proceedings of the 8th International Precision Engineering Seminar (IPES), (1995) 101-104.

[6] V. Badami, S. Patterson, A frequency domain method for the measurement of nonlinearity in heterodyne interferometry. Precision Engineering, 24(1), (2000) 41-49.

[7] V. Badami, S. Patterson, Investigation of nonlinearity in high-accuracy heterodyne laser interferometry. In Proceedings of the 12th annual American Society for Precision Engineering (ASPE) conference, (1997) 153-156.

[8] T. Schmitz, D.C. Chu, H.S. Kim, First and second order periodic error measurement for non-constant velocity motions. Precision Engineering, 33(4), (2009) 353-361.

[9] T. Schmitz, C. Adhia, H.S. Kim, Periodic error quantification for non-constant velocity motion. Precision Engineering, 36(1), (2012) 153-157.

[10] C. Lu, S.R. Gillmer, J.D. Ellis, T.L. Schmitz, J.R. Troutman, J.A. Tarbutton, Application of wavelet analysis in heterodyne interferometry. In Proceedings of the 28th annual American Society for Precision Engineering (ASPE) conference, (2013) 364-367.

[11] C. Lu, J.R. Troutman, J.D. Ellis, T.L. Schmitz, J.A. Tarbutton, Periodic error compensation using frequency measurement with continuous wavelet transform. In Proceedings of the 29th annual American Society for Precision Engineering (ASPE) conference, (2014) 408-411.

[12] C. Lu, J.D. Ellis, T.L. Schmitz, J.A. Tarbutton, Improvement of a periodic error compensation algorithm based on the continuous wavelet transform. In Proceedings of the 30th annual American Society for Precision Engineering (ASPE) conference, (2015).

[13] C. Lu, J.R. Troutman, T.L. Schmitz, J.D. Ellis, J.A. Tarbutton, Application of the continuous wavelet transform in periodic error compensation. Precision Engineering, 44, (2016) 245-251.

[14] I. Daubechies, The wavelet transform time-frequency localization and signal analysis. IEEE Transactions on Information Theory, 36, (1990) 961-1004.

[15] M. Farge, Wavelet transforms and their applications to turbulence. Annual Review of Fluid Mechanics, 24, (1992) 395-457.

[16] G. Kaiser, A friendly guide to wavelets, Birkhauser, 1994.

[17] H. Liu, A.N. Cartwright, C. Basaran, Moire interferogram phase extraction: a ridge detection algorithm for continuous wavelet transforms. Applied Optics, 15, (2004) 850-857.

[18] M. Cherbuliez, P. Jacquot, Phase computation through wavelet analysis: yesterday and nowadays. Fringe, (2001) 154-162.